

**Ab initio study of charge-transfer dynamics in collisions of C<sup>2+</sup> ions with hydrogen chloride**E. Rozsályi,<sup>1</sup> E. Bene,<sup>2</sup> G. J. Halász,<sup>3</sup> Á. Vibók,<sup>1</sup> and M. C. Bacchus-Montabonel<sup>4</sup><sup>1</sup>Department of Theoretical Physics, University of Debrecen, P.O. Box 5, H-4010 Debrecen, Hungary<sup>2</sup>Institute of Nuclear Research, Hungarian Academy of Sciences, P.O. Box 51, H-4001 Debrecen, Hungary<sup>3</sup>Department of Information Technology, University of Debrecen, P.O. Box 12, H-4010 Debrecen, Hungary<sup>4</sup>Laboratoire de Spectrométrie Ionique et Moléculaire, Université de Lyon (Lyon I), CNRS-UMR5579, 43 Bd. du 11 Novembre 1918, F-69622 Villeurbanne Cedex, France

(Received 22 March 2011; published 31 May 2011)

*Ab initio* quantum chemistry molecular calculations followed by a semiclassical dynamical treatment in the keV collision energy range have been developed for the study of the charge-transfer process in collisions of C<sup>2+</sup> ions with hydrogen chloride. The mechanism has been investigated in detail in connection with avoided crossings between states involved in the reaction. A simple mechanism driven by a strong nonadiabatic coupling matrix element has been pointed out for this process. A comparative analysis with the halogen fluoride target corresponding to a similar electronic configuration shows a quite different charge-transfer mechanism leading to a very different behavior of the cross sections. Such behavior may be correlated to specific nonadiabatic interactions observed in these collision systems.

DOI: [10.1103/PhysRevA.83.052713](https://doi.org/10.1103/PhysRevA.83.052713)

PACS number(s): 34.70.+e

**I. INTRODUCTION**

Important experimental and theoretical effort has been devoted recently in order to investigate collisions of slow multiply charged ions with molecular targets. These studies provide detailed analysis on electron capture processes occurring during the collision and on fragmentation dynamics of the ionized species after removal of electrons from the target. A special attention has been focused first on reactions with simple targets such as molecular hydrogen [1–4]. Great interest is now devoted to more complex molecular targets, diatomics [6,7,9], polyatomic molecules, and even biomolecular targets [10–16] in order to analyze the mechanisms involved at the molecular level.

In these reactions, removal of an electron from the molecular target by charge transfer may be considered as a first step, often followed by possible excitation and fragmentation of the molecule and detailed information on this initial process is determinant. Such electron exchange process may be studied in a molecular description of the collision. The molecular calculation is performed using *ab initio* quantum chemistry methods in order to determine potential-energy surfaces of the different states involved in the process and corresponding radial and rotational couplings. The collision dynamics may be derived in the keV energy range by means of semiclassical approaches. We have investigated the charge-transfer process in collisions of multicharged ions with hydrogen halide molecules. The C<sup>2+</sup> projectile ion has been chosen as in previous works in order to have a comparative analysis for a series of diatomics [6–9]. Hydrogen halide targets offer the advantage to lead to a relatively simple fragmentation pattern. Effectively, with regard to the relative atomic mass of hydrogen and halogen atoms, the fragments have very different kinetic energies and may be easily separated experimentally [5]. But it is important to have also a detailed description of the electron capture process. In a previous paper, the charge transfer in the C<sup>2+</sup> + HF collision has been studied [9]. A detailed analysis of the anisotropy of the collision process

with regard to the nonadiabatic interactions around avoided crossings between the molecular states involved in the process has been driven. Two main interactions have been pointed out for this process; one of them correlated to a short-range interaction between the two lowest charge-transfer levels, and the most important one to a longer-range interaction between the highest charge-transfer level and the entry channel. This interaction leads to an increase of the charge-transfer cross section at higher collision energies around  $E_{\text{lab}} = 100$  keV. The vibration of the molecular target has also been considered and the cross sections on the different vibration levels have been estimated in the Franck-Condon approximation. The work is now extended to the hydrogen chloride target corresponding to a similar electronic configuration, but a quite higher size and mass of the heteroatom. We would like to investigate the charge transfer in that case in comparison with the previous HF target, in particular to look at the efficiency of the charge-transfer process with regard to possible steric or electronic effects. A detailed analysis of the mechanism in each reaction, in connection with nonadiabatic interactions between molecular states involved, will also be performed.

**II. MOLECULAR CALCULATIONS**

The geometry of the system may be described by the internal Jacobi coordinates  $\{R, r, \theta\}$ . The origin is taken at the center of mass of the target molecule, which is almost on the chlorine atom with regard to the respective atomic mass of hydrogen and chlorine. As defined in Fig. 1, the collision of the C<sup>2+</sup> ion towards the hydrogen atom in the linear approach would correspond to the angle  $\theta = 0^\circ$  and the collision toward the chlorine atom to the geometry  $\theta = 180^\circ$ . The molecular calculations have been carried out using the MOLPRO suite of *ab initio* programs [17]. A pseudopotential has been used to take account of the core electrons of the chlorine atom. Different tests have been performed for the choice of this pseudopotential and the basis set of atomic orbitals. The ECP10sdf (Effective Core Potential

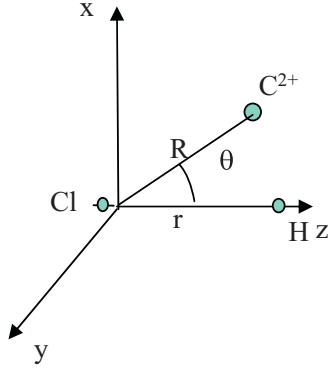


FIG. 1. (Color online) Internal coordinates for the  $C^{2+} - HCl$  collision system.

10 core-electron) relativistic pseudopotential has been used for chlorine [18] with the correlation-consistent aug-cc-pVTZ (augmented correlation-consistent polarized valence-triple-zeta) basis sets of Dunning [19]. The same basis set has been chosen for carbon and hydrogen atoms. Calculations have been performed using state-averaged CASSCF-MRCI (complete active space self-consistent field-multireference configuration interaction) methods. The active space includes the  $1s$  orbital of hydrogen, the  $n=2$  and  $n=3(sp)$  orbitals for carbon, and the  $n=3$  orbitals for chlorine, the core electrons being treated by a pseudopotential. The  $1s$  orbital of carbon has been frozen in the calculation. The geometry of the  $^1\Sigma^+$  ground state of HCl has been optimized at the CASSCF (complete active space self-consistent field) level of theory leading to an equilibrium distance  $r_{eq} = 1.2748 \text{ \AA}$  in good agreement with the experimental value  $1.2746 \text{ \AA}$  [20]. The corresponding vertical ionization potential calculated using MRCI (multireference configuration interaction) methods is  $12.69 \text{ eV}$ , to be compared to the experimental value  $12.748 \text{ eV}$  obtained from photoelectron spectra measurements [20,21]. The asymptotic energies of the  $C^{2+} - HCl$  molecular system may be compared to separated species calculations taking account of experimental ionization potentials and carbon ion levels [20–22] combined with MRCI calculations at optimized equilibrium geometry for the HCl and  $HCl^+$  ground and excited states. The calculated asymptotic energy difference between the entry channel and the highest  $^1\Sigma^+\{C^+(1s^2 2s^2 2p)^2 D + HCl^+(^2\Pi)\}$  exit channel is  $2.35 \text{ eV}$ , with a discrepancy of  $0.06 \text{ eV}$  with experimental data assuming a good description of both entry and exit channels. The asymptotic energy difference of the two lowest charge-transfer levels  $^1\Sigma^+\{C^+(1s^2 2s^2 2p)^2 P^\circ + HCl^+(^2\Pi)\}$  and  $^1\Sigma^+\{C^+(1s^2 2s^2 2p)^2 P^\circ + HCl^+(^2\Sigma^+)\}$  is  $4.15 \text{ eV}$ , in agreement with calculated separated species. The spin-orbit effects can be neglected in the collision energy range of interest so electron spin may be conserved in the collision process and only singlet states will be correlated to the  $^1\Sigma^+$  entry channel.

Charge-transfer processes are driven mainly by nonadiabatic interactions in the vicinity of avoided crossings [23,24], in particular between the entry channel and charge-transfer levels. The radial coupling matrix elements between all pairs of states of the same symmetry have

thus been calculated by means of the finite difference technique [25]:

$$g_{KL}(R) = \langle \psi_K | \partial / \partial R | \psi_L \rangle \\ = \langle \psi_K(R) | \lim_{\Delta \rightarrow 0} \frac{1}{\Delta} | \psi_L(R + \Delta) - \psi_L(R) \rangle,$$

which, taking account of the orthogonality of the eigenfunctions  $|\psi_K(R)\rangle$  and  $|\psi_L(R)\rangle$  for  $K \neq L$ , reduces to

$$g_{KL}(R) = \langle \psi_K | \partial / \partial R | \psi_L \rangle \\ = \lim_{\Delta \rightarrow 0} \frac{1}{\Delta} \langle \psi_K(R) | \psi_L(R + \Delta) \rangle.$$

The parameter  $\Delta$  has been tested and the value  $\Delta = 0.0012 \text{ a.u.}$  has been chosen as in previous calculations [26] using the three-point numerical differentiation method for reasons of numerical accuracy.

The interaction between  $^1\Sigma^+$  and  $^1\Pi$  states by means of rotational coupling has also been taken into account. The rotational coupling matrix elements  $\langle \psi_K(R) | iL_y | \psi_L(R) \rangle$  between states of angular momentum  $\Delta L = \pm 1$  have been calculated directly from the quadrupole moment tensor from the expression  $iL_y = x \frac{\partial}{\partial z} - z \frac{\partial}{\partial x}$  with the center of mass of the system as the origin of electronic coordinates [27].

Taking account of the  $^1\Sigma^+$  symmetry of the  $C^{2+}(1s^2 2s^2)S + HCl(^1\Sigma^+)$  entry channel, only  $C^+(^2P^\circ)$  or  $C^+(^2D)$  states could be involved in the collision process. Effectively,  $C^+(^4P)$  states could lead only to triplet and quintet states, which cannot be correlated to the entry channel as spin-orbit coupling is negligible. With regard to the different excited states of  $HCl^+$ , there are thus four  $^1\Sigma^+$  states, which can be correlated by means of radial coupling, the entry channel  $^1\Sigma^+\{C^{2+}(1s^2 2s^2)S + HCl(^1\Sigma^+)\}$  and three charge-transfer levels  $^1\Sigma^+\{C^+(1s^2 2s^2 2p)^2 P^\circ + HCl^+(^2\Pi)\}$ ,  $^1\Sigma^+\{C^+(1s^2 2s^2 2p)^2 P^\circ + HCl^+(^2\Sigma^+)\}$ ,  $^1\Sigma^+\{C^+(1s^2 2s^2 2p)^2 D + HCl^+(^2\Pi)\}$ . We have also to take into account the  $^1\Pi$  states, which can be correlated to the  $^1\Sigma^+$  entry channel by rotational coupling interaction; all charge-transfer levels may be concerned:  $^1\Pi\{C^+(1s^2 2s^2 2p)^2 P^\circ + HCl^+(^2\Pi)\}$ ,  $^1\Pi\{C^+(1s^2 2s^2 2p)^2 P^\circ + HCl^+(^2\Sigma^+)\}$ ,  $^1\Pi\{C^+(1s^2 2s^2 2p)^2 D + HCl^+(^2\Pi)\}$ . The corresponding potential-energy curves have been calculated in the  $[2.0-14.0] \text{ a.u.}$  internuclear distance range. They are presented in Fig. 2 for the equilibrium distance in the linear geometry. The main feature is a very strong avoided crossing between the  $^1\Sigma^+$  entry channel and the  $^3\Sigma^+\{C^+(1s^2 2s^2 2p)^2 D + HCl^+(^2\Pi)\}$  charge-transfer level around  $R = 11 \text{ a.u.}$  This avoided crossing appears to be the leading nonadiabatic interaction in the present  $C^{2+} + HCl$  collision system. The other avoided crossings, between  $^1\Sigma^+\{C^+(1s^2 2s^2 2p)^2 P^\circ + HCl^+(^2\Pi)\}$  and  $^2\Sigma^+\{C^+(1s^2 2s^2 2p)^2 P^\circ + HCl^+(^2\Sigma^+)\}$  exit channels, or between the  $^2\Sigma^+\{C^+(1s^2 2s^2 2p)^2 P^\circ + HCl^+(^2\Sigma^+)\}$  and  $^3\Sigma^+\{C^+(1s^2 2s^2 2p)^2 D + HCl^+(^2\Pi)\}$  levels, are significantly smoother and correspond to large energy gaps. They could certainly not be determinant in the process. Such a strong interaction between the entry channel and one charge-transfer level was not present in the  $C^{2+} + HF$  collision system. Effectively, in that case, the  $^3\Sigma^+\{C^+(1s^2 2s^2 2p)^2 D + HF^+(^2\Pi)\}$  level was higher in energy than the entry channel with regard to the ionization

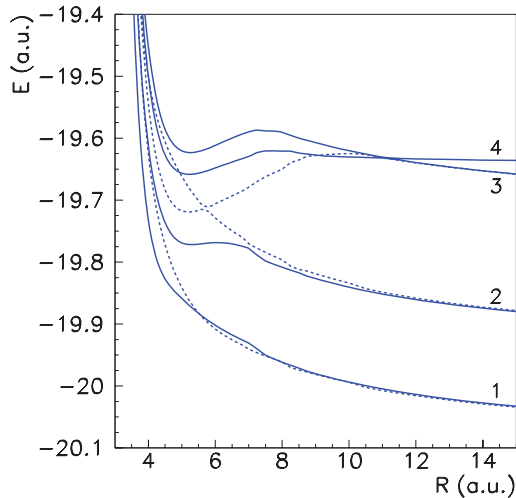


FIG. 2. (Color online) : Potential-energy curves for the  $^1\Sigma^+$  (full line) and  $^1\Pi$  (broken line) states of the  $C^{2+}-HCl$  molecular system at equilibrium,  $\theta = 0^\circ$ . 1:  $C^+(1s^22s^22p)^2P^\circ + HCl^+(^2\Pi)$ ; 2:  $C^+(1s^22s^22p)^2P^\circ + HCl^+(^2\Sigma^+)$ ; 3:  $C^+(1s^22s^22p)^2D + HCl^+(^2\Pi)$ ; 4:  $C^{2+}(1s^22s^2)^1S + HCl(^1\Sigma^+)$  entry channel.

potential of HF and could not be populated directly. So the only exit channel which could be accessible from the entry channel was the  $^1\Sigma^+\{C^+(1s^22s^22p)^2P^\circ + HF^+(^2\Sigma^+)\}$  showing a relatively smooth interaction around  $R = 6.5$  a.u., and of course the lowest  $^1\Sigma^+\{C^+(1s^22s^22p)^2P^\circ + HF^+(^2\Pi)\}$  charge-transfer state, which is certainly too low in energy to be determinant in the process. Another important feature to point out in the  $C^{2+} + HCl$  collision, always in tight connection with the existence of the  $\{C^+(1s^22s^22p)^2D + HCl^+(^2\Pi)\}$  exit channel, is the strong nonadiabatic interaction observed between the  $2^1\Pi\{C^+(1s^22s^22p)^2P^\circ + HCl^+(^2\Sigma^+)\}$  and  $3^1\Pi\{C^+(1s^22s^22p)^2D + HCl^+(^2\Pi)\}$  charge-transfer levels. This interaction was, of course, not present in the  $C^{2+} + HF$  collision system and could induce an increase of the rotational effect.

Such interactions may be visualized also on the radial and rotational coupling matrix elements. The most important features are presented in Figs. 3 and 4 respectively. The radial nonadiabatic coupling matrix element between the  $3^1\Sigma^+$  and the  $4^1\Sigma^+$  entry channel shows clearly a strong peak, 1.48 a.u. high, in correspondence to the very strong avoided crossing between the potential-energy curves. Such coupling is more than three times higher than the other radial couplings. Besides, the strong interaction between the  $2^1\Pi\{C^+(1s^22s^22p)^2P^\circ + HCl^+(^2\Sigma^+)\}$  and  $3^1\Pi\{C^+(1s^22s^22p)^2D + HCl^+(^2\Pi)\}$  exit channels pointed out on the potential-energy curves leads to a sharp crossing between rot22 and rot32 correlated to the change of character of the  $\Pi$  wave functions in the neighborhood of the avoided crossing. On the contrary, the interaction between states 1 and 2 being very smooth for both  $^1\Sigma^+$  and  $^1\Pi$  symmetries, the rotational coupling rot11 remains almost equal to 1 for all distances.

### III. COLLISION DYNAMICS

The collision treatment has been performed in the keV energy range. For energies higher than 10 eV/amu, straight-line

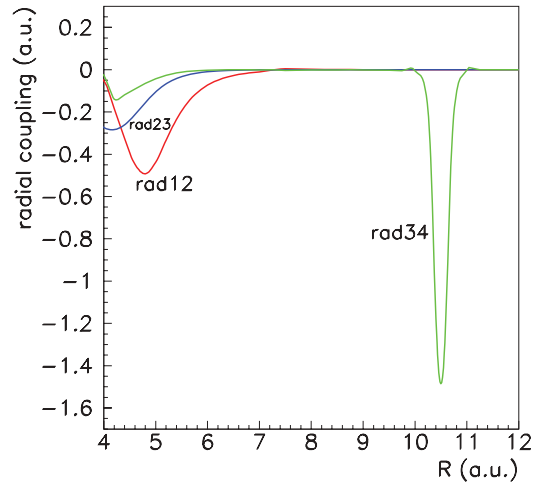


FIG. 3. (Color online) Radial coupling matrix elements between  $^1\Sigma^+$  states of the  $C^{2+}-HCl$  molecular system at equilibrium,  $\theta = 0^\circ$ . Same labels as in Fig. 2.

trajectories are satisfying [28] and semiclassical approaches may be applied with a good accuracy. The EIKONX code based on an efficient propagation method has been used [29]. In the collision process, electronic transitions are much faster than vibration and rotation motion so that the sudden approximation can be applied. The cross sections, corresponding to purely electronic transitions, are thus determined by solving the impact-parameter equation as in the usual ion-atom approach, considering the internuclear distance of the molecular target fixed in a given geometry. This simple model has been widely used in the field of ion-molecule collisions and leads to reliable results in the keV energy range we are dealing with [30,31].

The coupled equations have been solved taking account of all the molecular states involved in the process by means of the transitions driven by radial and rotational coupling matrix elements. Translation factors may be introduced so that cross

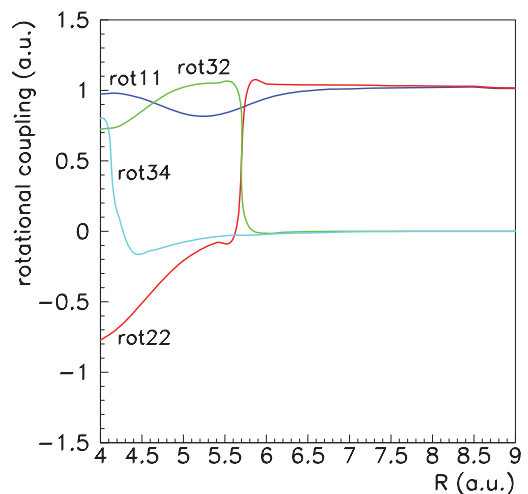


FIG. 4. (Color online) Rotational coupling matrix elements between  $^1\Sigma^+$  and  $^1\Pi$  states for the  $C^{2+}-HCl$  molecular system at equilibrium,  $\theta = 0^\circ$ . Same labels as in Fig. 2. rot11 =  $\langle 1^1\Pi | iLy | 1^1\Sigma^+ \rangle$ ; rot22 =  $\langle 2^1\Pi | iLy | 2^1\Sigma^+ \rangle$ ; rot32 =  $\langle 3^1\Pi | iLy | 2^1\Sigma^+ \rangle$ ; rot34 =  $\langle 3^1\Pi | iLy | 4^1\Sigma^+ \rangle$ .

sections would be independent of the origin of coordinates and to avoid spurious coupling terms at long range. They may be evaluated in the approximation of the common translation factors [32,33]. The radial and rotational coupling matrix elements are thus transformed respectively into

$$\langle \psi_K | \partial / \partial R - (\varepsilon_K - \varepsilon_L) z^2 / 2R | \psi_L \rangle$$

and

$$\langle \psi_K | iL_y + (\varepsilon_K - \varepsilon_L) zx | \psi_L \rangle,$$

Where  $\varepsilon_K$  and  $\varepsilon_L$  are the electronic energies of states  $|\psi_K\rangle$  and  $|\psi_L\rangle$ ,  $z^2$  and  $zx$ , the components of the quadrupole moment tensor. Such effect has been tested for the  $C^{2+} + HF$  collision system in the [3–108]-keV laboratory energy range ([0.1–0.6]-a.u. collision velocity range). The corresponding cross sections are presented in Fig. 5. The introduction of translation factors induces a very small variation on the total cross sections, less than 3% at  $E_{lab} = 100$  keV. The effect decreases at lower collision energies and is completely negligible below about 30 keV. Such effect depends of course of the collision system, but, in a first approach, it can be considered with a good approximation to be weak in the energy range we are dealing with and has not been taken into account in the  $C^{2+} + HCl$  collision treatment.

The partial and total cross sections are presented in Fig. 6 and Table I for the linear C-H-Cl geometry ( $\theta = 0^\circ$ ). The total cross section presents a peak around  $v_{coll} = 0.1$  a.u. ( $E_{lab} = 3$  keV) and then decreases at higher collision energy. Such a peak is mainly due to the contribution of the corresponding peak of the partial cross section sec43. As pointed out from the potential-energy curves, the charge-transfer process appears clearly dominated by one nonadiabatic in-

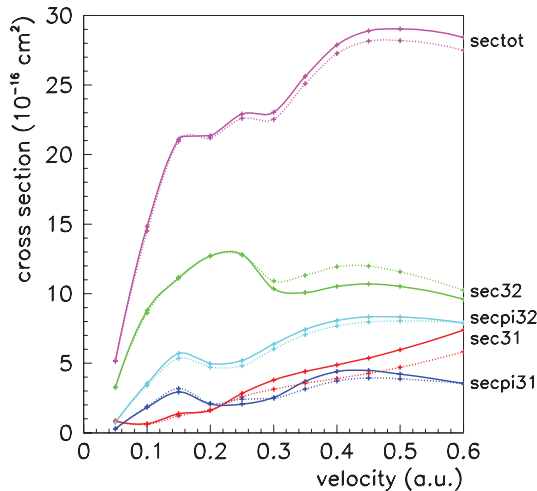


FIG. 5. (Color online) Total and partial charge-transfer cross sections for the  $C^{2+} - HF$  collision system at equilibrium,  $\theta = 0^\circ$ . Full line: with translation factors; broken line: without translation factors. sectot: total cross section; sec32: partial cross section on  ${}^1\Sigma^+\{C^+(1s^22s^22p)^2P^\circ + HF^+({}^2\Sigma^+)\}$ ; secpi32: partial cross section on  ${}^1\Pi\{C^+(1s^22s^22p)^2P^\circ + HF^+({}^2\Sigma^+)\}$ ; sec31, partial cross section on  ${}^1\Sigma^+\{C^+(1s^22s^22p)^2P^\circ + HF^+({}^2\Pi)\}$ ; secpi31: partial cross section on  ${}^1\Pi\{C^+(1s^22s^22p)^2P^\circ + HF^+({}^2\Pi)\}$ .

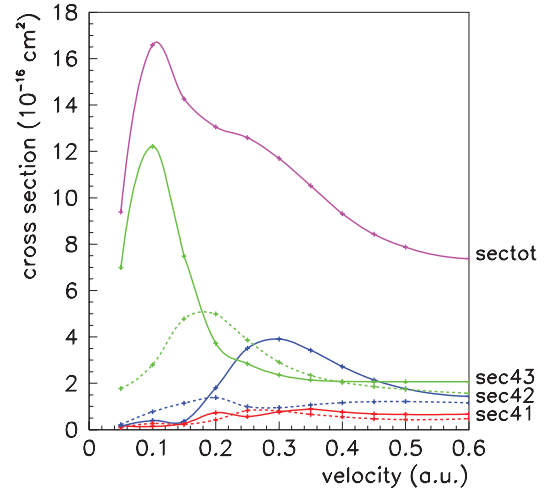


FIG. 6. (Color online) Total and partial charge-transfer cross sections for the  $C^{2+} - HCl$  collision system at equilibrium,  $\theta = 0^\circ$ . Full line: transition to  ${}^1\Sigma^+$  states; broken line: transition to  ${}^1\Pi$  states. sectot: total cross section; sec43: partial cross section on  $\{C^+(1s^22s^22p)^2D + HCl^+({}^2\Pi)\}$ ; sec42: partial cross section on  $\{C^+(1s^22s^22p)^2P^\circ + HCl^+({}^2\Sigma^+)\}$ ; sec41: partial cross section on  ${}^1\Sigma^+\{C^+(1s^22s^22p)^2P^\circ + HCl^+({}^2\Pi)\}$ .

teraction corresponding to the avoided crossing between the entry channel and the highest  $3^1\Sigma^+\{C^+(1s^22s^22p)^2D + HCl^+({}^2\Pi)\}$  charge-transfer level, which gives rise to the strong peak of the partial cross section sec43. The shorter-range crossing between  $3^1\Sigma^+\{C^+(1s^22s^22p)^2D + HCl^+({}^2\Pi)\}$  and  $2^1\Sigma^+\{C^+(1s^22s^22p)^2P^\circ + HCl^+({}^2\Sigma^+)\}$  channels is also involved in the  $C^{2+} + HCl$  charge-transfer process; it leads in particular to a hump in the sec42 partial cross section, but its contribution is largely lower than the strong interaction between the entry channel and the  $3^1\Sigma^+\{C^+(1s^22s^22p)^2D + HCl^+({}^2\Pi)\}$  charge-transfer channel. Such behavior is completely different from the mechanism observed in the  $C^{2+} + HF$  collision system where the  ${}^1\Sigma^+, {}^1\Pi\{C^+(1s^22s^22p)^2D + HF^+({}^2\Pi)\}$  exit channel could not be accessible. The charge-transfer process was thus driven by shorter-range crossings, in particular between the entry channel and the  $2^1\Sigma^+\{C^+(1s^22s^22p)^2P^\circ + HF^+({}^2\Sigma^+)\}$  exit channel around  $R = 6.5$  a.u. and a competition with the avoided crossing with the lowest  ${}^1\Sigma^+\{C^+(1s^22s^22p)^2P^\circ + HF^+({}^2\Pi)\}$  charge-transfer level was observed [9]. These interactions were leading, at variance from the  $C^{2+} + HCl$  collision, to an increase of the charge-transfer cross sections at higher energies around  $E_{lab} = 100$  keV and the charge transfer appears more efficient in the collision of  $C^{2+}$  ions with HF than with the HCl target (Table I).

As already pointed out for  $C^{2+} + HF$ , rotational effects may be observed also for this system as charge-transfer channels may be all correlated to the entry channel by means of rotational coupling. In particular, a hump is shown on the partial cross section on the  $2^1\Pi\{C^+(1s^22s^22p)^2P^\circ + HCl^+({}^2\Sigma^+)\}$  exit channel in connection with the nonadiabatic interaction between the  $2^1\Pi\{C^+(1s^22s^22p)^2P^\circ + HCl^+({}^2\Sigma^+)\}$  and  $3^1\Pi\{C^+(1s^22s^22p)^2D + HCl^+({}^2\Pi)\}$  charge-transfer levels pointed out in the molecular calculations. However, the

TABLE I. Charge-transfer cross sections for the  $C^{2+} + HCl$  collision system (in  $10^{-16} \text{ cm}^2$ ). Comparison with the  $C^{2+} + HF$  collision system. Same labels as in Fig. 2.

Velocity (a.u.)	$E_{lab}$ (keV)	sec43 $4^1\Sigma^+3^1\Sigma^+$	secpi43 $4^1\Sigma^+3^1\Pi$	sec42 $4^1\Sigma^+2^1\Sigma^+$	secpi42 $4^1\Sigma^+2^1\Pi$	sec41 $4^1\Sigma^+1^1\Sigma^+$	secpi41 $4^1\Sigma^+1^1\Pi$	Sectot $C^{2+}+HCl$	Sectot $C^{2+}+HF$
0.05	0.75	6.99	1.78	0.14	0.22	0.17	0.09	9.38	10.54
0.1	3	12.22	2.80	0.39	0.77	0.14	0.27	16.58	14.22
0.15	6.75	7.48	4.78	0.36	1.14	0.27	0.23	14.26	16.10
0.2	12	3.73	4.99	1.80	1.38	0.73	0.42	13.05	16.64
0.25	18.75	2.84	3.86	3.50	0.99	0.57	0.82	12.59	17.89
0.3	27	2.36	2.91	3.91	0.95	0.77	0.81	11.70	19.10
0.35	36.75	2.14	2.34	3.43	1.07	0.88	0.66	10.52	20.51
0.4	48	2.08	2.03	2.72	1.16	0.77	0.55	9.32	21.49
0.45	60.75	2.07	1.86	2.14	1.21	0.68	0.47	8.42	22.01
0.5	75	2.06	1.74	1.77	1.21	0.65	0.43	7.87	22.20
0.6	108	2.07	1.57	1.44	1.15	0.67	0.48	7.37	22.23

contribution of  $^1\Pi$  exit channels decreases at higher collision energies, and is almost of the same order of magnitude as the contribution of corresponding  $^1\Sigma^+$  charge-transfer states coupled by radial coupling (Table I). The mechanism of the  $C^{2+} + HCl$  charge transfer is clearly dominated by the nonadiabatic radial coupling interaction rad34. On the contrary, rotational effects remain significant in  $C^{2+} + HF$  at higher collision energies, in particular for the  $2^1\Pi\{C^+(1s^22s^22p)^2P^o + HF^+(^2\Sigma^+)\}$  channel, and contribute significantly to the total cross section.

#### IV. CONCLUDING REMARKS

We have presented a theoretical treatment of charge-transfer processes induced by collision of the  $C^{2+}$  projectile on hydrogen chloride. This reaction may be compared to the  $C^{2+} + HF$  collision system involving a quite similar molecular target. Different features may be observed for these collision systems. They do not appear to rely on possible steric effects, but more likely to the electronic interactions in the vicinity of avoided crossings. In  $C^{2+} + HCl$ , the charge transfer is driven essentially by the nonadiabatic radial coupling interaction between the entry channel and the highest  $3^1\Sigma^+\{C^+(1s^22s^22p)^2D + HCl^+(^2\Pi)\}$  charge-transfer channel. The total cross section presents a maximum of  $16.6 \times 10^{-16} \text{ cm}^2$  around  $E_{lab} = 3 \text{ keV}$  and decreases at higher energies. The mechanism is

completely different for the  $C^{2+} + HF$  collision system. In that case, the  $\{C^+(1s^22s^22p)^2D + HF^+(^2\Pi)\}$  charge-transfer channel cannot be accessible directly from the entry channel. A two crossing mechanism is observed, mainly driven by the interaction at shorter range with the  $\{C^+(1s^22s^22p)^2P^o + HF^+(^2\Sigma^+)\}$  exit channel leading to important values of the total cross section at higher collision energy by contribution of radial coupling with a significant rotational effect [9]. The charge transfer is globally more efficient with the HF molecular target with total cross sections from  $14.2 \times 10^{-16} \text{ cm}^2$  at  $E_{lab} = 3 \text{ keV}$  to about  $22.0 \times 10^{-16} \text{ cm}^2$  at  $E_{lab} = 100 \text{ keV}$ . These comparative results show clearly that the charge-transfer mechanism is fundamentally dependent of the specific nonadiabatic interactions involved in each collision system. General conclusions for a series of molecular targets, even of similar electronic configurations, have to be handled with care and the analysis of the behavior of each molecular system is essential.

#### ACKNOWLEDGMENTS

This work was granted access to the HPC resources of [CCRT/CINES/IDRIS under the allocation 2011-(i2011081655) made by GENCI (Grand Equipement National de Calcul Intensif) as well as from COST actions CM0702 CUSPFEL and MP1002 Nano-IBCT.

[1] P. Sobocinski, J. Rangama, G. Laurent, L. Adoui, A. Cassimi, J.-Y. Chesnel, A. Dubois, D. Hennecart, X. Husson, and F. Frémont, *J. Phys. B* **35**, 1353 (2002).  
 [2] D. M. Kearns, R. W. McCullough, and H.B. Gilbody, *J. Phys. B* **35**, 4335 (2002).  
 [3] R. E. Olson and C. R. Feeler, *J. Phys. B* **34**, 1163 (2001).  
 [4] M. C. Bacchus-Montabonel, *Phys. Rev. A* **59**, 3569 (1999).  
 [5] F. Frémont, D. Martina, O. Kamalou, P. Sobocinski, J.-Y. Chesnel, I. R. McNab, and F. R. Bennett, *Phys. Rev. A* **71**, 042706 (2005).  
 [6] E. Bene, Á. Vibók, G. J. Halász, and M. C. Bacchus-Montabonel, *Chem. Phys. Lett.* **455**, 159 (2008).  
 [7] E. Bene, P. Martínez, G. J. Halász, Á. Vibók, and M. C. Bacchus-Montabonel, *Phys. Rev. A* **80**, 012711 (2009).  
 [8] M. C. Bacchus-Montabonel and Y. S. Tergiman, *Chem. Phys. Lett.* **497**, 18 (2010).  
 [9] E. Rozsályi, E. Bene, G. J. Halász, Á. Vibók, and M. C. Bacchus-Montabonel, *Phys. Rev. A* **81**, 062711 (2010).  
 [10] R. Cabrera-Trujillo, E. Deumens, Y. Ohrn, O. Quinet, J. R. Sabin, and N. Stolterfoht, *Phys. Rev. A* **75**, 052702 (2007).

- [11] F. Alvarado, S. Bari, R. Hoekstra, and T. Schlathöler, *J. Chem. Phys.* **127**, 034301 (2007).
- [12] J. de Vries, R. Hoekstra, R. Morgenstern, and T. Schlathöler, *Phys. Rev. Lett.* **91**, 053401 (2003).
- [13] M. C. Bacchus-Montabonel, M. Łabuda, Y. S. Tergiman, and J. E. Sienkiewicz, *Phys. Rev. A* **72**, 052706 (2005).
- [14] M. C. Bacchus-Montabonel and Y. S. Tergiman, *Phys. Rev. A* **74**, 054702 (2006).
- [15] M. C. Bacchus-Montabonel, Y. S. Tergiman, and D. Talbi, *Phys. Rev. A* **79**, 012710 (2009).
- [16] M. C. Bacchus-Montabonel and Y.S. Tergiman, *Chem. Phys. Lett.* **503**, 45 (2011).
- [17] MOLPRO (version 2009.1) is a package of *ab initio* programs written by H.-J. Werner *et al.*
- [18] A. Nicklass, M. Dolg, H. Stoll, and H. Preuss, *J. Chem. Phys.* **102**, 8942 (1995).
- [19] D. E. Woon and T. H. Dunning Jr., *J. Chem. Phys.* **98**, 1358 (1993).
- [20] K. P. Huber and G. Herzberg, in *Molecular Spectra and Molecular Structure IV. Constants of Diatomic Molecules* (Van Nostrand, Reinhold, New York, 1979).
- [21] A. A. Wills, D. Čubrić, M. Ukai, F. Currell, B. J. Goodwin, T. Reddish, and J. Comer, *J. Phys. B* **26**, 2601 (1993).
- [22] NIST Atomic Spectra Database Levels Data, [<http://www.nist.gov/pml/data/asd.cfm>]
- [23] B. Lasorne, M. C. Bacchus-Montabonel, N. Vaeck, and M. Desouter-Lecomte, *J. Chem. Phys.* **120**, 1271 (2004).
- [24] M. Gargaud, F. Fraija, M. C. Bacchus-Montabonel, and R. McCarroll, *J. Phys. B* **27**, 3985 (1994).
- [25] M. C. Bacchus-Montabonel, R. Cimiraglia, and M. Persico, *J. Phys. B* **17**, 1931 (1984).
- [26] M. C. Bacchus-Montabonel, C. Courbin, and R. McCarroll, *J. Phys. B* **24**, 4409 (1991).
- [27] M. C. Bacchus-Montabonel and F. Fraija, *Phys. Rev. A* **49**, 5108 (1994).
- [28] B. H. Bransden and M. R. C. McDowell, in *Charge Exchange and the Theory of Ion-Atom Collisions* (Clarendon, Oxford, 1992), pp. 63–64.
- [29] R. J. Allan, C. Courbin, P. Salas, and P. Wahnou, *J. Phys. B* **23**, L461 (1990).
- [30] D. R. Bates and R. McCarroll, *Proc. R. Soc. London, Ser. A* **245**, 175 (1958).
- [31] P. C. Stancil, B. Zygelman, and K. Kirby, in *Photonic, Electronic, and Atomic Collisions*, edited by F. Aumayr and H. P. Winter (World Scientific, Singapore, 1998), p. 537.
- [32] L. F. Errea, L. Méndez, and A. Riera, *J. Phys. B* **15**, 101 (1982).
- [33] F. Fraija, A. R. Allouche, and M. C. Bacchus-Montabonel, *Phys. Rev. A* **49**, 272 (1994).